

Ab initio calculation of H + He⁺ charge-transfer cross sections for plasma physicsJ. Loreau,^{1,*} K. Sodoga,^{2,3} D. Lauvergnat,² M. Desouter-Lecomte,^{2,4} and N. Vaeck¹¹*Laboratoire de Chimie Quantique et Photophysique, Université Libre de Bruxelles, CP 160/09 50, avenue F. D. Roosevelt, B-1050 Bruxelles, Belgium*²*Laboratoire de Chimie Physique, Bâtiment 349, Université de Paris-Sud, UMR8000, F-91405 Orsay, France*³*Faculté des Sciences, Département de Physique, Université de Lomé, Boîte Postale 1515 Lomé, Togo*⁴*Département de Chimie, B6c, Université de Liège, Sart-Tilman, B-4000 Liège 1, Belgium*

(Received 28 April 2010; published 26 July 2010)

The charge-transfer in low-energy (0.25 to 150 eV/amu) H(*nl*) + He⁺(1s) collisions is investigated using a quasimolecular approach for the $n = 2, 3$ as well as the first two $n = 4$ singlet states. The diabatic potential energy curves of the HeH⁺ molecular ion are obtained from the adiabatic potential energy curves and the nonadiabatic radial coupling matrix elements using a two-by-two diabaticization method, and a time-dependent wave-packet approach is used to calculate the state-to-state cross sections. We find a strong dependence of the charge-transfer cross section on the principal and orbital quantum numbers n and l of the initial or final state. We estimate the effect of the nonadiabatic rotational couplings, which is found to be important even at energies below 1 eV/amu. However, the effect is small on the total cross sections at energies below 10 eV/amu. We observe that to calculate charge-transfer cross sections in an n manifold, it is only necessary to include states with $n' \leq n$, and we discuss the limitations of our approach as the number of states increases.

DOI: [10.1103/PhysRevA.82.012708](https://doi.org/10.1103/PhysRevA.82.012708)

PACS number(s): 34.70.+e, 52.20.Hv

I. INTRODUCTION

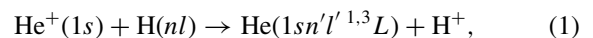
Starting with the historical work of Massey and Smith in 1933 [1], and due to the apparent simplicity of this two-electron system, the asymmetrical charge-transfer process He(1s²1S) + H⁺ → H + He⁺ was quickly considered a prototype for semiclassical methods to treat collisions [2–6]. This process is dominated by the capture into the H(1s) state, but later the charge-transfer excitation and the direct excitation processes were studied in detail both theoretically and experimentally [7–15]. All these reactions require an intermediate collision energy, for which a semiclassical description is perfectly suited. This is also true for the charge-transfer mechanism which involves an H⁻ ion as projectile, He²⁺ + H⁻ → H + He⁺(*nl*) [16,17].

At a much lower collisional energy, charge-transfer can populate excited states of He(1s*nl*^{1,3}L) from the corresponding excited states *nl* of H. Although there is no measurement for those processes, they have been studied theoretically using a semiclassical approach with a linear trajectory for the nuclei, taking into account the coupling between the initial Stark splitting H states and the final He states at large internuclear distances ($R \geq 20$ a.u.) and neglecting electron translational factors and rotational couplings [18,19]. These works provide data for an energy range between 2.5 and 10 keV/amu.

Recently, it has appeared that those low-energy charge-transfer processes involving excited hydrogen states could be of major importance for the monitoring of warm plasmas [20]. Indeed, spectroscopic methods are among the most effective approaches for determining particle transport in magnetically confined fusion plasmas. From this point of view, the simulation of excited He emissions resolved in

space and time has been proposed as a tool independent of the theoretical plasma model. Atomic physics simulations can be compared to experimental data, and the diffusion and convective velocity parameters can be determined. However, the He⁺ ions will interact with the H-D background via a charge-transfer mechanism which modifies the population of the He excited states and, therefore, the intensity of the emission lines. A self-consistent approach to the description of the coupling of the radiating He with the plasma background via charge-transfer has shown that these processes are very important at low collisional energies (typically of the order of 0.1 to 100 eV) and that, therefore, an accurate knowledge of charge-transfer cross sections in this energy range is essential [20].

In this work, we have adopted a quasimolecular approach to the ion-atom collision based on the use of quantum chemistry *ab initio* methods to obtain the potential energy curves (PECs) as well as the radial and rotational coupling matrix elements of the quasimolecule HeH⁺. A wave-packet method is used to treat the curve-crossing dynamics resulting from the failure of the Born-Oppenheimer approximation [21,22]. A Gaussian wave packet is prepared in the entrance channel and propagated on the coupled ro-electronic channels. The collision matrix elements are computed from an analysis of the flux in the asymptotic region by using properties of absorbing potentials, giving access to the charge-transfer cross sections for the processes



where $n, n' = 2-3$. The cross sections for the inverse process, He(1s*n'l'*^{1,3}L) + H⁺ → He⁺(1s) + H(*nl*), can be obtained by a detailed balance analysis of reaction (1).

Finally, we estimate the influence of the rotational couplings on the cross sections.

*jloreau@ulb.ac.be

II. THEORY

A. Molecular data

The Hamiltonian is given as the sum of an electronic part and a nuclear kinetic part:

$$H = T^N + H^{\text{el}}. \quad (2)$$

The electronic Hamiltonian includes a kinetic term for the electrons and all the potential energy terms.

The PECs $U_{m\Lambda}$ and the adiabatic electronic functions $\zeta_{m\Lambda}$ solve the equation for the electronic motion:

$$H^{\text{el}}\zeta_{m\Lambda}(\mathbf{r}; R) = U_{m\Lambda}(R)\zeta_{m\Lambda}(\mathbf{r}; R), \quad (3)$$

where \mathbf{r} stands for the electron coordinates and R is the radial coordinate for the nuclei. m is used to number the states for a given value of Λ , the quantum number associated with L_z . L_z is the projection of the total electronic orbital angular momentum \mathbf{L} onto the molecular z axis, chosen along the radial nuclear coordinate R . Molecular electronic states are classified according to the value of $|\Lambda|$: Σ states correspond to $\Lambda = 0$, Π states to $|\Lambda| = 1$, and Δ states to $|\Lambda| = 2$. We therefore see that states with $|\Lambda| \neq 0$ are doubly degenerate for singlet states. In the atomic limit ($R \rightarrow \infty$), Λ becomes m_L , the magnetic quantum number.

In contrast, T^N can be written in atomic units as the sum of a radial part,

$$H^{\text{rad}} = -\frac{1}{2\mu} \partial_R^2, \quad (4)$$

where μ is the reduced mass of the system, and a rotational part, given by

$$\begin{aligned} H^{\text{rot}} &= \frac{1}{2\mu R^2} \mathbf{N}^2 \\ &= \frac{1}{2\mu R^2} (\mathbf{K}^2 + \mathbf{L}^2 - 2K_z L_z - K_+ L_- - K_- L_+), \end{aligned} \quad (5)$$

where \mathbf{N} is the nuclear angular momentum. In this work, we focus on singlet states and we do not consider any spin-dependent interactions, so that the total angular momentum is $\mathbf{K} = \mathbf{N} + \mathbf{L}$. Since $T^N = H^{\text{rad}} + H^{\text{rot}}$, the nuclear wave function is the product of a radial part and an angular part: $\psi_{m\Lambda}(\mathbf{R}) = \psi_{m\Lambda}(R) |K\Lambda M\rangle$, where M is the eigenvalue of L_z , the projection of \mathbf{L} onto the laboratory Z axis. The angular functions are eigenfunctions of \mathbf{K}^2 and K_z with eigenvalues $K(K+1)$ and Λ , respectively (the eigenvalues of L_z and K_z are identical, as \mathbf{N} is perpendicular to the z axis). The action of the ladder operators $K_{\pm} = K_x \pm iK_y$ is given by $K_{\pm} |K\Lambda M\rangle = [K(K+1) - \Lambda(\Lambda \mp 1)]^{1/2} |K\Lambda \mp 1 M\rangle$.

In the basis of these electronic-rotational functions, the matrix elements of H^{rot} are given by

$$\begin{aligned} H_{m\Lambda K, m'\Lambda' K'}^{\text{rot}} &= \frac{1}{2\mu R^2} \{ [K(K+1) - \Lambda^2] \delta_{mm'} \delta_{\Lambda\Lambda'} - (L_-)_{mm'} \\ &\quad \times [K(K+1) - \Lambda(\Lambda-1)]^{1/2} \delta_{\Lambda, \Lambda'-1} - (L_+)_{mm'} \\ &\quad \times [K(K+1) - \Lambda(\Lambda+1)]^{1/2} \delta_{\Lambda, \Lambda'+1} \} \delta_{KK'}, \end{aligned} \quad (6)$$

where the contribution from $(L_x^2 + L_y^2)_{mm'} \delta_{\Lambda\Lambda'}$ has been neglected. We see that states with $\Delta\Lambda = \pm 1$ will interact through the rotational Hamiltonian.

To treat the effects of the rotational Hamiltonian, it is more convenient to work with parity adapted functions [23]. These functions are defined by

$$\begin{aligned} |mK\Lambda M\epsilon\rangle &= \frac{1}{\sqrt{2+2\delta_{\Lambda 0}}} [|K\Lambda M\rangle \zeta_{m\Lambda} \\ &\quad + (-1)^K \epsilon |K-\Lambda M\rangle \zeta_{m-\Lambda}], \end{aligned} \quad (7)$$

where $\epsilon = 1$ and $\epsilon = -1$ correspond to e and f states, respectively. Using (6) and (7), it can be shown that H^{rot} only connects states of the same parity. As $^1\Sigma^+$ states can have e or f symmetry, only half the Π states must be taken into account in the calculations.

We consider here the $n = 1-3$ $^1\Sigma^+$, $^1\Pi$, and $^1\Delta$ states as well as the first two $n = 4$ $^1\Sigma^+$ states. We could not include more $n = 4$ states in the calculations, as we were not able to calculate the radial nonadiabatic couplings between these states by *ab initio* methods. The dissociative atomic states and the asymptotic energies of the molecular states are reported in Table I. We have also considered the $n = 2$ $^3\Sigma^+$ and $^3\Pi$ states to allow comparison with [18] and [19] (see Sec. III F). The adiabatic PECs for these states have been calculated using the *ab initio* quantum chemistry package MOLPRO, version 2006.1 [24]. An adapted basis set consisting of the aug-cc-pv5Z basis set [25] supplemented by one contracted Gaussian function per orbital per atom up to $n = 4$ has been used. Details of the calculations are given in [26]. In Tables 1–6 of [26], the dissociative wave functions of the

TABLE I. CASSCF energies at $R = 50$ a.u. and dissociative products of the singlet states included in the calculations.

$^{2S+1}\Lambda$	n	m	Energy (hartree) at $R = 50$ a.u.	Atomic products
$^1\Sigma^+$	1	1	-2.8980	He($1s^2\ ^1S$) + H $^+$
		2	-2.4999	He $^+(1s)$ + H($1s$)
	2	3	-2.1448	He($1s2s\ ^1S$) + H $^+$
		4	-2.1262	He $^+(1s)$ + H($2p$)
		5	-2.1238	He $^+(1s)$ + H($2s$)
	3	6	-2.1226	He($1s2p\ ^1P^o$) + H $^+$
		7	-2.0623	He($1s3s\ ^1S$) + H $^+$
		8	-2.0600	He $^+(1s)$ + H($3d$)
		9	-2.0568	He($1s3d\ ^1D$) + H $^+$
		10	-2.0552	He $^+(1s)$ + H($3p$)
		11	-2.0528	He($1s3p\ ^1P^o$) + H $^+$
	4	12	-2.0523	He $^+(1s)$ + H($3s$)
		13	-2.0421	He($1s4s\ ^1S$) + H $^+$
		14	-2.0330	He $^+(1s)$ + H($4p$)
$^1\Pi$	2	1	-2.1249	He $^+(1s)$ + H($2p$)
		2	-2.1235	He($1s2p\ ^1P^o$) + H $^+$
	3	3	-2.0571	He $^+(1s)$ + H($3d$)
		4	-2.0567	He($1s3d\ ^1D$) + H $^+$
		5	-2.0536	He $^+(1s)$ + H($3p$)
		6	-2.0532	He($1s3p\ ^1P^o$) + H $^+$
$^1\Delta$	3	1	-2.0554	He $^+(1s)$ + H($3d$)
		2	-2.0554	He($1s3d\ ^1D$) + H $^+$

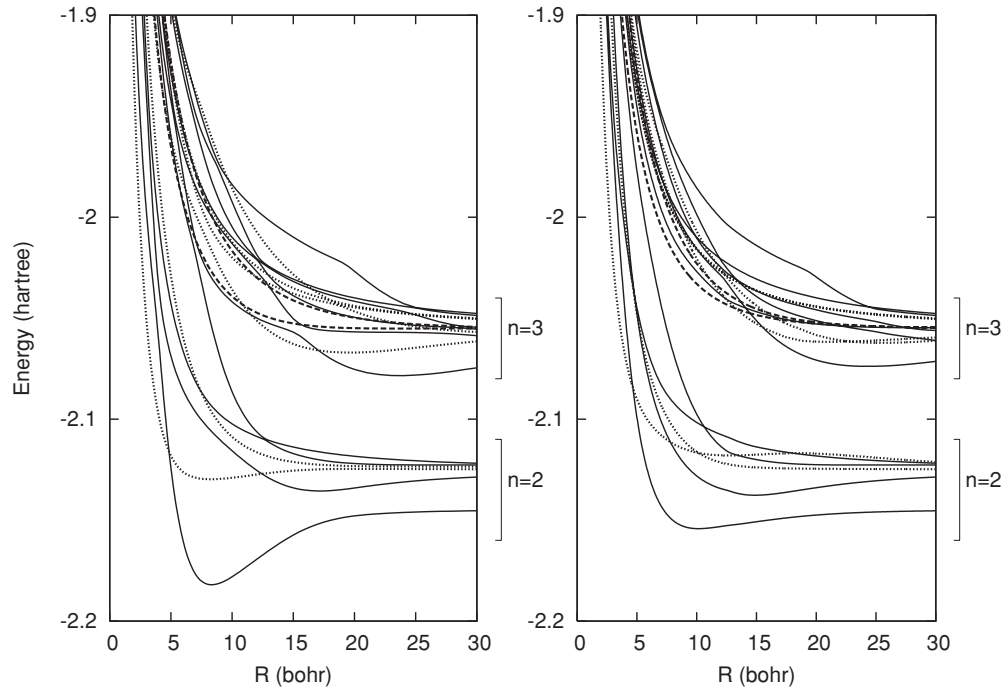


FIG. 1. Adiabatic (left) and diabatic (right) PECs of the $n = 2, 3$ states of HeH^+ . Solid lines, $^1\Sigma^+$ states; dotted lines, $^1\Pi$ states; dashed lines, $^1\Delta$ states. $n = 1$ $^1\Sigma^+$ states have been excluded from the diabaticization procedure.

hydrogen states are expressed as a linear combination of the atomic states. This results from the electric field produced by $\text{He}^+(1s)$, which induces a Stark mixing of the hydrogen states. However, these Stark states adiabatically become pure atomic states as $R \rightarrow \infty$ so that we know with certainty the atomic configuration corresponding to a molecular state, as indicated in Table I. For example, the fourth and fifth states in the $^1\Sigma^+$ symmetry dissociate into $\text{H}(2p)$ and $\text{H}(2s)$, respectively.

The PECs have been calculated at the state-averaged complete active space self-consistent field (CASSCF) level and are shown in Fig. 1 for the $n = 2-3$ states. This approach allows us to compute the radial nonadiabatic coupling matrix elements $F_{m\Lambda, m'\Lambda} = \langle \zeta_{m\Lambda} | \partial_R | \zeta_{m'\Lambda} \rangle$, which are used to build the diabatic representation [27]. The adiabatic-to-diabatic transformation matrix \mathbb{D} is the solution to the differential matrix equation $\partial_R \mathbb{D} + \mathbb{F} \cdot \mathbb{D} = 0$ and the diabatic PECs are the diagonal elements of the matrix $\mathbb{U}^d = \mathbb{D}^{-1} \cdot \mathbb{U} \cdot \mathbb{D}$, where \mathbb{U} is the matrix of H^{el} in the adiabatic representation. We have used an approximate \mathbb{F} matrix by keeping only the couplings between adjacent states, that is, the elements $F_{m, m+1}$. The main reason is that this approach simplifies the diabaticization procedure considerably [26]. It has been shown to give results similar to those obtained when the complete \mathbb{F} matrix is taken into account in dynamical calculations [28], something we have also observed in the low-energy calculation of the charge-transfer cross sections for the $n = 2$ $^1\Sigma^+$ states (see the following). These PECs and nonadiabatic couplings were also used to estimate the photodissociation cross section of HeH^+ [29].

The nonadiabatic rotational coupling matrix elements $\langle \zeta_{m\Lambda} | L_{\pm} | \zeta_{m'\Lambda'} \rangle$ appearing in Eq. (6) have also been computed at the CASSCF level using MOLPRO, with the origin of coordinates at the nuclear center of mass. As pointed out in [26]

[30], and [31], some of these couplings behave asymptotically as R , a phenomenon that cannot be avoided by changing the origin of electronic coordinates. Due to the factor $1/R^2$ in Eq. (6), these couplings will thus decrease as $1/R$, much more slowly than the radial couplings, which decrease to 0 extremely rapidly outside the interaction region. This causes a problem in the calculation of the cross sections, as it implies the use of very large numerical grids that increase the calculation time tremendously. To solve this problem, we modified the problematic rotational couplings outside the interaction region, where we required that they decrease to 0 (i.e., their atomic values). We have tried various switching functions to find a set of parameters that had no effect on the cross sections. This approximation is also justified in our case by the fact that the linear rotational couplings usually connect two states in the same atomic configuration, so that the modification will not influence the charge-transfer cross sections.

There are also cases where the atomic value of $\langle \zeta_{m\Lambda} | L_{\pm} | \zeta_{m'\Lambda'} \rangle$ is a constant but not 0. The rotational Hamiltonian then decreases as $1/R^2$, which still implies the use of large numerical grids. However, this can only happen again for transitions between two states in the same atomic configuration (electron excitation), a process we do not consider here.

In the atomic limit, when the nonadiabatic rotational couplings are neglected, our method implies conservation of the magnetic quantum number m_L as the Hamiltonian is diagonal in Λ . When they are included in the calculations, we have interaction between states with $\Delta m_L = 0, \pm 1$.

B. Cross-section calculation

The cross section corresponding to the transfer of an electron from an initial state m, Λ to a final state m', Λ' is

given by [32]

$$\sigma_{m'\Lambda',m\Lambda}(E) = \frac{\pi}{k_{m\Lambda}^2(E)} \sum_K (2K+1) \times |S_{m'\Lambda',m\Lambda}^K(E) - \delta_{m'm}\delta_{\Lambda'\Lambda}|^2, \quad (8)$$

where $k_{m\Lambda}$ is the wave number in the entrance channel, $k_{m\Lambda} = \sqrt{2\mu(E - U_{m\Lambda})}$. As the Hamiltonian is diagonal in K [see Eq. (6)], the cross section must be calculated for each value of K until convergence in Eq. (8).

We use the coupled-channel formalism in the rotational-electronic diabatic representation. In the time-dependent formalism, we start by defining a Gaussian initial wave packet which is propagated in time using the split-operator algorithm [33]. The coupled equations give access to the wave packets on all the rotational-electronic states. For each value of K , the scattering matrix elements $|S_{m'\Lambda',m\Lambda}^K(E)|^2$ are then extracted using the flux operator formalism with a complex absorbing potential [34,35].

We start by defining the functions

$$\Phi_{m\Lambda,E}^{\pm,K} = \sqrt{\frac{\mu}{2\pi k_{m\Lambda}}} h_K^{\pm}(k_{m\Lambda}R) \zeta_{m\Lambda}^d, \quad (9)$$

where $h_K^{\pm}(k_{m\Lambda}R)$ are the Riccati-Hankel functions [36] and $\zeta_{m\Lambda}^d$ are the electronic wave functions in the diabatic representation.

We then introduce the time-independent energy normalized wave functions $|\Psi_{m\Lambda,E}^{+,K}\rangle$, solutions of

$$\left(-\frac{1}{2\mu} \partial_R^2 + \frac{1}{2\mu R^2} [K(K+1) - \Lambda^2] + H^{\text{el}} \right) |\Psi_{m\Lambda,E}^{+,K}\rangle = U_{m\Lambda} |\Psi_{m\Lambda,E}^{+,K}\rangle \quad (10)$$

and satisfying the asymptotic condition

$$|\Psi_{m\Lambda,E}^{+,K}\rangle \xrightarrow{R \rightarrow \infty} |\Phi_{m\Lambda,E}^{-,K}\rangle - \sum_{m'\Lambda'} S_{m'\Lambda',m\Lambda}^K(E) |\Phi_{m'\Lambda',E}^{+,K}\rangle. \quad (11)$$

These stationary eigenfunctions can be constructed as the Fourier transform of a time-dependent wave packet $\Phi(t)$:

$$|\Psi_{m\Lambda,E}^{+,K}\rangle = \frac{1}{2\pi \Gamma_{m\Lambda}^K(E)} \int_{-\infty}^{+\infty} |\Phi_{m\Lambda}(t)\rangle \exp(iEt) dt. \quad (12)$$

The vector $|\Phi(t)\rangle$ is constructed by propagating an initial wave packet $|\Phi(0)\rangle$ in time using the Hamiltonian matrix in the rotational-electronic diabatic representation:

$$|\Phi(t)\rangle = \exp(-i\mathbb{H}^d t) |\Phi(0)\rangle. \quad (13)$$

The initial wave packet is 0 except in the diabatic channel $m\Lambda$, where it is represented by a Gaussian function $g(R)$ of width σ and centered around R_0 :

$$g(R) = \frac{1}{\sqrt{\sigma} \sqrt{2/\pi}} \exp\left(ik_0 R - \frac{(R - R_0)^2}{\sigma^2} \right). \quad (14)$$

$\Gamma_{\Lambda m}^K$ is the amplitude of the initial wave packet on the stationary states:

$$\Gamma_{m\Lambda}^K = \langle \Psi_{m\Lambda,E}^{+,K} | \Phi_0 \rangle = \sqrt{\frac{\mu}{2\pi k_{m\Lambda}}} \int_0^{\infty} h_K^+(k_{m\Lambda}R) g(R) dR. \quad (15)$$

The flux operator is defined by [34]

$$F = -\frac{i}{2\mu} \left(\frac{\partial}{\partial R} \delta(R - R_c) + \delta(R - R_c) \frac{\partial}{\partial R} \right), \quad (16)$$

where R_c is a point in the asymptotic region (i.e., such that there is no interaction for $R \geq R_c$) located behind R_0 .

Using Eqs. (9), (11), and (16), one arrives at

$$\langle \Psi_{m\Lambda,E}^{+,K} | F | \Psi_{m\Lambda,E}^{+,K} \rangle = \frac{1}{2\pi} \sum_{m'\Lambda'} |S_{m'\Lambda',m\Lambda}^K(E)|^2. \quad (17)$$

The sum can be removed using the projector onto the electronic state $m'\Lambda'$, $P_{m'\Lambda'} = |\zeta_{m'\Lambda'}^d\rangle \langle \zeta_{m'\Lambda'}^d|$, to obtain

$$\langle \Psi_{m\Lambda,E}^{+,K} | P_{m'\Lambda'} F P_{m'\Lambda'} | \Psi_{m\Lambda,E}^{+,K} \rangle = \frac{1}{2\pi} |S_{m'\Lambda',m\Lambda}^K(E)|^2. \quad (18)$$

A complex absorbing potential (CAP) $-iW$ is then added to the Hamiltonian, which becomes $H' = H - iW$. The left-hand side of Eq. (18) is then calculated using Eqs. (12) and (13) with H' instead of H . This is allowed if the CAP is “switched on” in the asymptotic region: in the interaction region, the CAP vanishes and the values of $\Phi(t)$ propagated with H or H' will be identical. Combining Eqs. (12) and (18), we find that the state-to-state cross section is given by

$$|S_{m'\Lambda',m\Lambda}^K(E)|^2 = \frac{1}{2\pi |\Gamma_{m\Lambda}^K(E)|^2} \int_0^{\infty} dt \int_0^{\infty} dt' \langle \Phi(t) | P_{m'\Lambda'} \times W P_{m'\Lambda'} | \Phi(t') \rangle \exp[iE(t' - t)]. \quad (19)$$

Equation (19) is used to obtain the matrix elements of S .

In our calculations, we used a CAP given by

$$W(R) = \eta_c \frac{(R - R_c)^2}{R_{\infty} - R_c}, \quad (20)$$

where η_c is the strength of the CAP and R_{∞} is the last point of the grid.

III. CHARGE-TRANSFER CROSS SECTIONS

A. Computational details

The calculations presented in this work were performed on the HP-XC 4000 cluster at the VUB/ULB computing center.

1. Parameters for dynamics

The parameters are chosen so as to ensure convergence of the sum in Eq. (8) while keeping the norm of the S matrix close to unity. For calculations involving the $n = 2$ states, a typical set of parameters consists of 2^{12} points for a grid of 60 a.u., an initial wave packet located around $R_0 = 40$ a.u. of width $\sigma = 0.2$, and a CAP starting at $R_c = 45$ a.u. of strength $\eta_c = 0.01$. The time needed for the wave packet to return to the asymptotic region obviously depends on the collision energy. For the preceding set of parameters, it is approximately contained between 2×10^3 and 3×10^4 a.u. for energies between 100 and 0.2 eV/amu. The computational time is approximately independent of the energy and is of the order of 1 h on 16 processors.

For calculations of cross sections involving $n = 3$ states, we had to use grids up to $R = 100$ a.u. This is due to the fact that the number of avoided crossings increases strongly with

n , so that the positions of the radial nonadiabatic couplings are shifted to larger internuclear distances [26]. The time needed for the wave packet to return to the asymptotic region is therefore increased and can be as high as 5×10^4 a.u. for low energies. The computational time depends on the number of states considered (see Sec. III B) and is of the order of 15 h on 16 processors.

When the rotational couplings are included in the calculations, the convergence of the partial cross sections is considerably slower as a function of K . It is therefore necessary to use much larger grids, and as a consequence, the time of propagation is increased tremendously. In addition, the number of points of the grid must also be increased to keep a constant step dR , again extending the computational time. To reduce the calculation time, we used grids of variable size, ranging from 150 a.u. for small K to 600 a.u. for values of K around 2500. When treating the $n = 3$ states, we could not perform calculations of partial cross sections for energies higher than 10 eV/amu, as even these large grids did not ensure convergence. The width of the wave packet was also increased up to $\sigma = 1.5$ for these large grids, as wave packets with a larger width stay more compact. In this case, the computational time can reach several days on 16 processors.

2. Nonadiabatic radial couplings

The first result that needs to be established is the validity of our approximation which consists in retaining only the nonadiabatic radial couplings $F_{m,m+1}$ instead of the complete \mathbb{F} matrix. We show in Fig. 2 a comparison between the two methods in the calculation of cross sections for the process $\text{H}(2s) + \text{He}^+(1s) \rightarrow \text{H}^+ + \text{He}(1s2l^1L)$. We conclude that this approximation is perfectly valid at low energies but that small deviations are observed at higher energies, $E \sim 100$ eV/amu. The same conclusion is reached for the cross section for the process $\text{H}(2p) + \text{He}^+(1s) \rightarrow \text{H}^+ + \text{He}(1s2l^1L)$.

Another issue is the fact that due to the Stark effect on hydrogen, some PECs undergo avoided crossings at large internuclear distances. However, as pointed out in [26], the high amplitude and the narrowness of the nonadiabatic radial

couplings at those points indicate that a full diagonal diabatic representation at the crossing is perfectly justified, so that these crossings will not affect the cross sections.

Finally, as pointed out in [26], the effect of the electron translation factors was found to be negligible in the range of energy considered in this work.

B. General observations

From a practical viewpoint, the calculation time of a cross section goes roughly as $e^{0.3m}$, where m is the number of states included in the calculations, so that the computing time doubles every time two additional states are considered. This again extends the computational time when rotational interactions are taken into account, as Σ and Π states must be considered in the same calculation. It is therefore important to take the fewest states possible, and we will see that states with different values of n can be considered independently.

A few things seem to come out from our cross-section calculations, which are presented here. The first is that, to a good degree of precision, the charge-transfer cross sections in a given n manifold are not modified by the inclusion of states with a principal quantum number $n' \neq n$, a fact illustrated in Fig. 3 for the $n = 2$ $^1\Sigma^+$ states. It was anticipated that the $n = 1$ states did not play any role in the $n > 1$ cross sections since they are much lower in energy, but the possibility of treating the $n = 2$ and $n = 3$ states separately was much less obvious. Indeed, the shape of the diabatic PEC is strongly influenced by the inclusion of states with different principal quantum numbers, and the density of states increases with n [26]. We reached the same conclusion for the influence of the first two $n = 4$ states on the $n = 3$ manifold and in the $^1\Pi$ symmetry.

However, while the cross section from the $n = 2$ onto the $n = 1$ states is always negligible, this is not the case in general, as the states interact through nonadiabatic radial couplings. For example, the cross sections from the $n = 3$ onto the $n = 2$

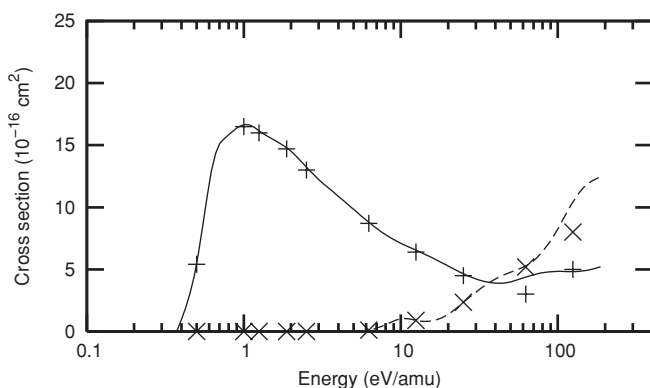


FIG. 2. Comparison of the two-by-two diabaticization with the use of the complete \mathbb{F} matrix in the calculation of charge-transfer cross sections with $\text{He}^+(1s) + \text{H}(2s)$ in the $^1\Sigma^+$ symmetry as the initial state. Solid line and plus signs: charge-transfer onto $\text{He}(1s2p^1P^o) + \text{H}^+$ with a two-by-two or complete \mathbb{F} matrix, respectively. Dashed line and crosses: charge-transfer onto $\text{He}(1s2s^1S) + \text{H}^+$ with a two-by-two or complete \mathbb{F} matrix, respectively.

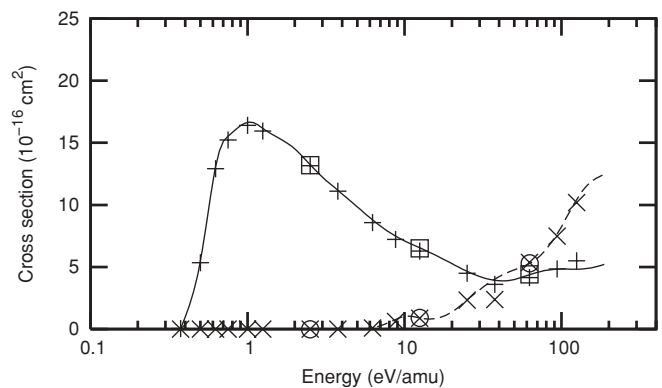


FIG. 3. Illustration of the possibility of treating states in different n manifolds independently in the calculation of charge-transfer cross sections with $\text{He}^+(1s) + \text{H}(2s)$ in the $^1\Sigma^+$ symmetry as the initial state. Solid line: charge-transfer onto $\text{He}(1s2p^1P^o) + \text{H}^+$ using the four $n = 2$ states. Plus signs: the same, but with the two $n = 1$ states included. Squares: the same, but with the six $n = 3$ states included. Dashed line: charge-transfer onto $\text{He}(1s2s^1S) + \text{H}^+$ using the four $n = 2$ states. Crosses: the same, but with the two $n = 1$ states included. Circles: the same, but with the six $n = 3$ states included.

states is not negligible, although the cross sections inside the $n = 3$ manifold are not modified by the inclusion of the $n = 2$ states. This means that the cross sections onto the $n = 2$ states result from a decrease in the elastic cross section.

The second observation is that there is a dependence of the cross section on n . This dependence was expected since the cross section scales classically as n^4 for Rydberg states. Finally, we also observed that, in an n manifold, the cross section always increases with the orbital quantum number l of the initial state.

C. $n = 2$ states

Cross sections with $H(2p)$ and $H(2s)$ in the Σ symmetry as well as $H(2p)$ in the Π symmetry as initial states are presented in Fig. 4. The behavior of the cross section for the process $H(2p) + He^+(1s) \rightarrow He(1s2p) + H^+$ is completely different in the Σ [Fig. 4(b)] and Π [Fig. 4(c)] symmetry: the total cross section from $H(2p)$ will be governed by the Π states at low energy and by the Σ states at high energy ($E \geq 100$ eV/amu). Another difference is the behavior of the cross section when the rotational couplings are included in the calculations: they have no effect for the transition with $H(2p) + He^+(1s)$ in the Σ symmetry as the initial state but strongly modify the cross section for the corresponding Π state. The cross section between the two Π states is decreased, while the cross section from Π to Σ states is increased so that the total cross section with $H(2p) + He^+(1s)$ as the initial state is roughly the same as when the rotational couplings were neglected.

The transition $H(2s) + He^+(1s) \rightarrow He(1s2p) + H^+$ is also affected by the inclusion of the rotational couplings at energies $E \geq 10$ eV/amu [Fig. 4(a)]. However, in this case the cross section between Σ states and from Σ to Π states are both increased. This simply means that for this state, the elastic cross section is decreased by the inclusion of rotational couplings.

D. $n = 3$ states

There are 12 $n = 3$ states. The cross section between the six $^1\Sigma^+$ states, presented in Figs. 5, 6, and 7, have been calculated including the $n = 2$ states since the cross section from the $n = 3$ to the $n = 2$ states is not negligible, as shown in the figures. There are also four $n = 3$ $^1\Pi$ states and two $^1\Delta$ states. The charge-transfer cross sections between these states are not presented here but are available as supplementary material [37], along with all the cross sections presented throughout this article. From these figures, it is clear that there is a dependence of the cross section on the principal and orbital quantum numbers, n and l , of the initial $H(nl)$ state: the charge-transfer cross section is much larger for $n = 3$ than for $n = 2$ and, also, increases with the value of l . The other difference between the $n = 2$ and the $n = 3$ manifolds is the influence of rotational couplings. While in the $n = 2$ states they were not influential at energies $E \leq 10$ eV/amu, this is not the case for the $n = 3$ states, where they play an important part even at energies below 1 eV/amu. We observe the intuitive fact that the cross sections between Σ states are smaller when the rotational interactions are taken into account, corresponding

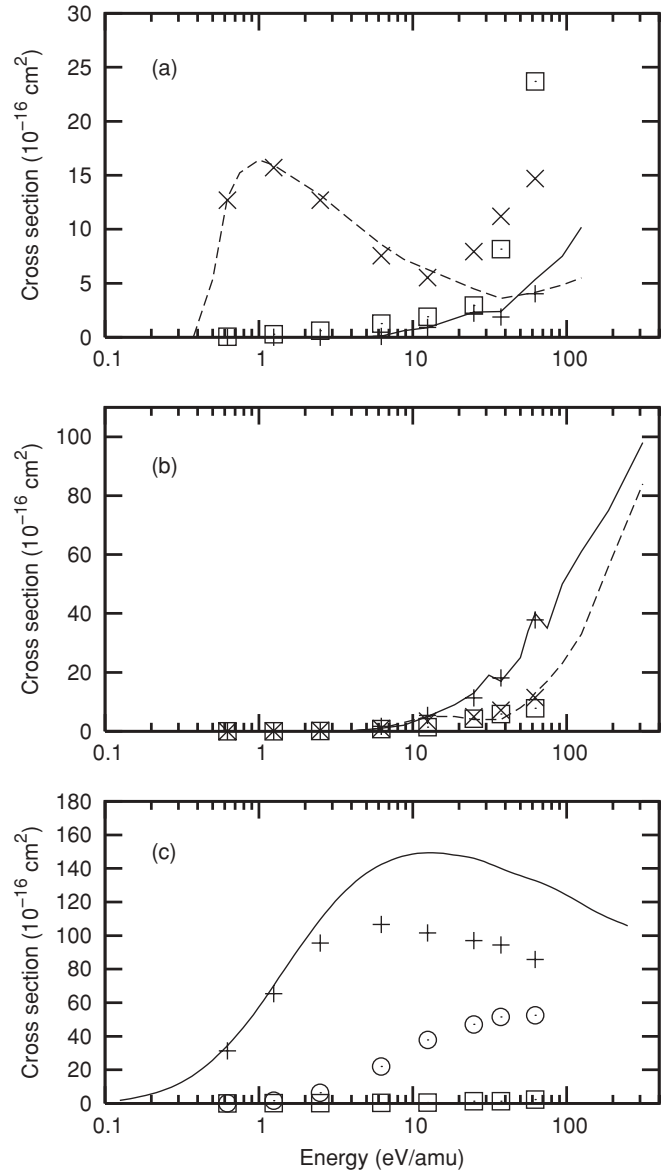


FIG. 4. Charge-transfer cross sections between the $n = 2$ states. (a) With $He^+(1s) + H(2s)$, $^1\Sigma^+$, as the initial state. Solid line: charge-transfer onto $He(1s2s\ ^1S) + H^+$, $^1\Sigma^+$. Plus signs: the same, but with rotational couplings. Dashed line: charge-transfer onto $He(1s2p\ ^1P^o) + H^+$, $^1\Sigma^+$. Crosses: the same, but with rotational couplings. Squares: charge-transfer onto $He(1s2p\ ^1P^o)$, $^1\Pi$. (b) The same as (a), but with $He^+(1s) + H(2p)$, $^1\Sigma^+$, as the initial state. (c) With $He^+(1s) + H(2p)$, $^1\Pi$, as the initial state. Solid line: charge-transfer onto $He(1s2p\ ^1P^o) + H^+$, $^1\Pi$. Plus signs: the same, but with rotational couplings. Squares: charge-transfer onto $He(1s2s\ ^1S) + H^+$, $^1\Sigma^+$. Circles: charge-transfer onto $He(1s2p\ ^1P^o) + H^+$, $^1\Sigma^+$.

to the fact that a part of the cross section is transferred onto the Π states.

We also observe that the cross sections onto the $He(1s2p\ ^1P^o) + H^+$ state in the Σ symmetry is smaller when the initial state is higher in energy. The cross section to the other $n = 2$ states, $He(1s2s\ ^1S) + H^+$ in the Σ symmetry and $He(1s2p\ ^1P^o) + H^+$ in the Π symmetry, are negligible and therefore not shown. Interestingly, the charge-transfer cross

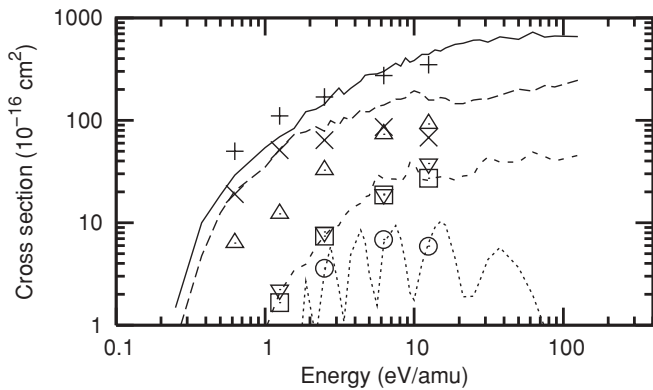


FIG. 5. Charge-transfer cross sections with He⁺(1s) + H(3d), ¹Σ⁺, as the initial state. Solid line: charge-transfer onto He(1s3s ¹S) + H⁺, ¹Σ⁺. Plus signs: the same, but with rotational couplings. Dashed line: charge-transfer onto He(1s3d ¹D) + H⁺, ¹Σ⁺. Crosses: the same, but with rotational couplings. Light dashed line: charge-transfer onto He(1s3p ¹P^o) + H⁺, ¹Σ⁺. Squares: the same, but with rotational couplings. Dotted line: charge-transfer onto He(1s2p ¹P^o) + H⁺, ¹Σ⁺. Circles: the same, but with rotational couplings. Triangles: charge-transfer onto He(1s3d ¹D) + H⁺, ¹Π. Inverted triangles: charge-transfer onto He(1s3p ¹P^o) + H⁺, ¹Π.

sections from the *n* = 2 states onto the *n* = 3 states are all negligible.

E. *n* = 4 states

We have included the first two *n* = 4 singlet states in the Σ symmetry. We could not consider more than the first two *n* = 4 states in the diabaticization since we were not able to calculate the radial nonadiabatic couplings for the higher-lying states. We calculated the cross section starting from the second *n* = 4 state, H(4p) + He⁺(1s). It confirms, once again, the dependence of the cross section in the quantum number *n* for a given value of *l*. We also observe that the cross sections from

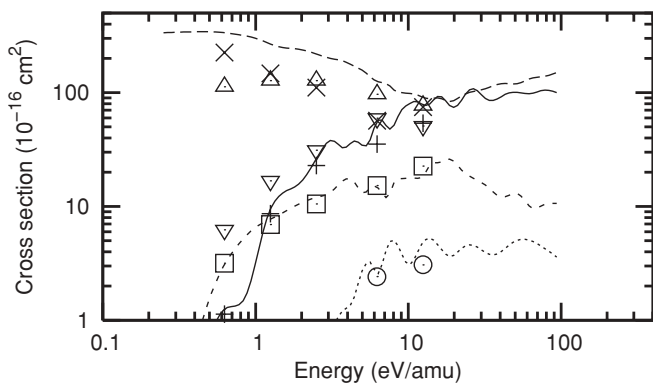


FIG. 6. Charge-transfer cross sections with He⁺(1s) + H(3p), ¹Σ⁺, as the initial state. Solid line: charge-transfer onto He(1s3s ¹S) + H⁺, ¹Σ⁺. Plus signs: the same, but with rotational couplings. Dashed line: charge-transfer onto He(1s3d ¹D) + H⁺, ¹Σ⁺. Crosses: the same, but with rotational couplings. Light dashed line: charge-transfer onto He(1s3p ¹P^o) + H⁺, ¹Σ⁺. Squares: the same, but with rotational couplings. Dotted line: charge-transfer onto He(1s2p ¹P^o) + H⁺, ¹Σ⁺. Circles: the same, but with rotational couplings. Triangles: charge-transfer onto He(1s3d ¹D) + H⁺, ¹Π. Inverted triangles: charge-transfer onto He(1s3p ¹P^o) + H⁺, ¹Π.

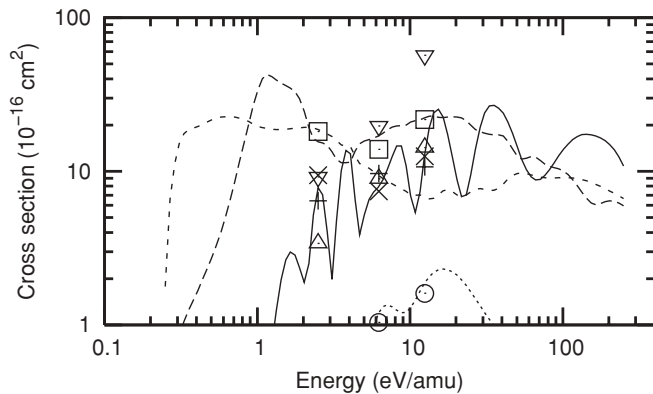


FIG. 7. Charge-transfer cross sections with He⁺(1s) + H(3s), ¹Σ⁺, as the initial state. Solid line: charge-transfer onto He(1s3s ¹S) + H⁺, ¹Σ⁺. Plus signs: the same, but with rotational couplings. Dashed line: charge-transfer onto He(1s3d ¹D) + H⁺, ¹Σ⁺. Crosses: the same, but with rotational couplings. Light dashed line: charge-transfer onto He(1s3p ¹P^o) + H⁺, ¹Σ⁺. Squares: the same, but with rotational couplings. Dotted line: charge-transfer onto He(1s2p ¹P^o) + H⁺, ¹Σ⁺. Circles: the same, but with rotational couplings. Triangles: charge-transfer onto He(1s3d ¹D) + H⁺, ¹Π. Inverted triangles: charge-transfer onto He(1s3p ¹P^o) + H⁺, ¹Π.

this *n* = 4 state onto the *n* = 3 states are not negligible, as shown in Fig. 8.

Moreover, it is observed (not shown) that despite the fact that the *n* = 3 and *n* = 4 states are close in energy and interact through radial nonadiabatic couplings, the cross sections in the *n* = 3 manifold are not influenced by these two *n* = 4 states, with the exception of the cross section with H(3s) + He⁺(1s) as the initial state, which is slightly modified at energies higher than 10 eV/amu. In addition, the cross section from H(3s) into the first *n* = 4 state, He(1s4s) + H⁺, is negligible. We thus reach the same conclusion as in the case of the *n* = 3 states: the cross sections from the *n* = 3 states onto the *n* = 2 states are not negligible, although they do not influence the cross section within the *n* = 2 manifold.

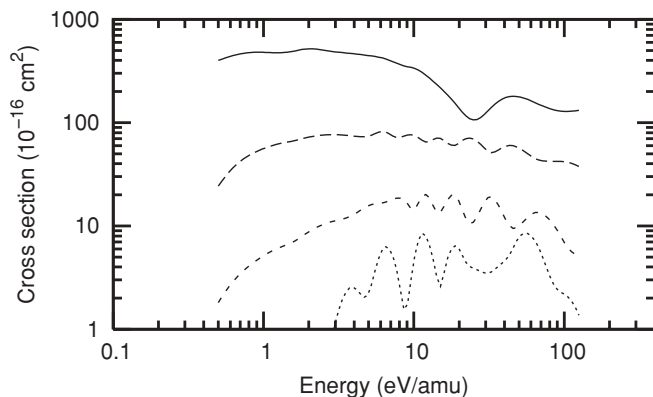


FIG. 8. Charge-transfer cross sections with He⁺(1s) + H(4p), ¹Σ⁺, as the initial state. Solid line: charge-transfer onto He(1s4s ¹S) + H⁺, ¹Σ⁺. Dashed line: charge-transfer onto He(1s3p ¹P^o) + H⁺, ¹Σ⁺. Light dashed line: charge-transfer onto He(1s3d ¹D) + H⁺, ¹Σ⁺. Dotted line: charge-transfer onto He(1s3s ¹S) + H⁺, ¹Σ⁺.

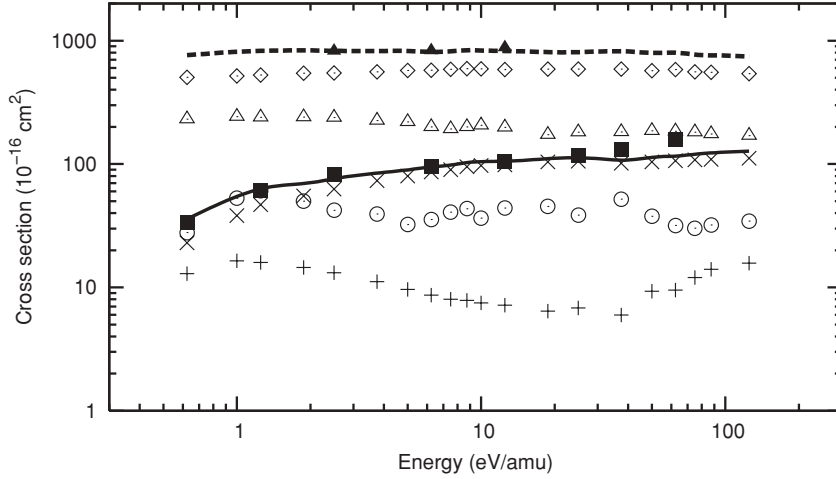


FIG. 9. Total charge-transfer cross sections starting from $H(nl) + He^+(1s)$. Plus signs, $H(2s)$; crosses, $H(2p)$; solid line, $H(n=2)$; filled squares $H(n=2)$ with rotational couplings. Circles, $H(3s)$; triangles, $H(3p)$; diamonds, $H(3d)$; dashed line, $H(n=3)$; filled triangles, $H(n=3)$ with rotational couplings.

In conclusion, it thus seems that the calculations of the charge-transfer cross sections within a given n manifold require to take into account only the states with $n' \leq n$.

F. Total cross sections

The total cross sections starting from a given nl state of H are obtained by summing all the contributions from within a Λ manifold,

$$\sigma(nl\Lambda) = \sum_{n'=1}^{\infty} \sum_{l'=0}^{n'-1} \sigma(nl\Lambda \rightarrow n'l'\Lambda), \quad (21)$$

and then by summing the contributions from all the Λ [19]:

$$\sigma(nl) = \frac{1}{2l+1} \sum_{\Lambda=-l}^l \sigma(nl\Lambda). \quad (22)$$

It should be noted that as the states with $\Lambda \neq 0$ are doubly degenerate, they contribute twice to the sum in Eq. (22). When the rotational couplings are taken into account, the only difference is an additional sum over Λ' in Eq. (21).

The total cross sections from the $H(nl)$ states, with $n = 2, 3$, are shown in Fig. 9 on a log-log scale. This figure clearly illustrates the dependence of the charge-transfer cross section in n and l . It also shows that while the inclusion of rotational couplings modifies the behavior of state-to-state cross sections at low energy, it modifies only slightly the total charge-transfer cross section of a n manifold. At energies higher than 10 eV/amu, the influence of rotational couplings starts to be important and the total cross section is increased. It would therefore be interesting to investigate the contributions of the rotational couplings at higher energies for $n = 3$ states, but it is clear that our method is not adapted to such calculations.

In the same way, we can determine the total cross section with the $He(1snl^1L) + H^+$ state as the final state. In helium-based plasma diagnostics, correct estimation of the populations of the various $He(1snl^{1,3}L)$ levels, which are modified by charge-transfer, is necessary. States such as $He(1snp^1P^o)$ decay radiatively to the ground state, and these emission lines can be observed. In Fig. 10 we have grouped together the charge-transfer cross sections with $He(1s2p^{1,3}P^o) + H^+$ and $He(1s3p^1P^o) + H^+$ as the final states, averaged over the

initial states. Interestingly, the conclusions are similar when we consider the sum of all cross sections into a specific final state and when we considered a specific initial state: we again see a dependence on n , which is now the principal quantum number of the helium atom. We also see that the influence of the rotational couplings is weak at low energies but that the total charge-transfer cross section is increased at energies ≥ 10 eV/amu.

These results can be compared with those of Chibisov *et al.* [19]. To describe the charge-transfer process, these authors used a semiclassical method with an atomic basis where only the Stark couplings between the atomic states are taken into account, and without rotational couplings. The cross section with $He(1s2p)$ as the final state ([19], Fig. 3) can be compared in the range of energy between 2.5 and 200 eV/amu (see Fig. 10). For the singlet states, we see not only that the behavior at low energies is different, but also that the cross section is several times smaller in our calculations. In the triplet symmetry, the orders of magnitude of the cross sections are roughly the same, but the general behavior is different. The comparison can also be made for the $n = 3$ states for Σ , Π , and

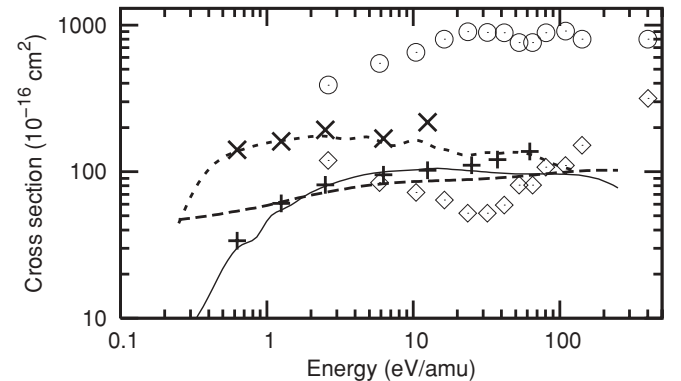


FIG. 10. Charge-transfer cross sections with $He(1s2p^{1,3}P^o) + H^+$ and $He(1s3p^1P^o) + H^+$ as the final state and comparison with [19]. Solid line: $He(1s2p^1P^o) + H^+$ as the final state. Plus signs: the same, but with rotational couplings. Dashed lines: $He(1s2p^3P^o) + H^+$ as the final state. Light dashed line: $He(1s3p^1P^o) + H^+$ as the final state. Crosses: the same, but with rotational couplings. Circles and diamonds: calculations from [19] for the singlet and triplet states, respectively. Points were extracted graphically.

Δ symmetries. In [18], Chibisov *et al.* present state-to-state cross-section calculations, so that the comparison with our calculations is direct. The results are again qualitatively very different, showing the limitations of their method.

IV. CONCLUSIONS

Using a quasimolecular approach and a wave-packet propagation method, we have computed the state-to-state cross sections for the charge-transfer collisional process $H(nl) + \text{He}^+(1s) \rightarrow \text{He}(1sn'l'{}^1L') + \text{H}^+$ for all the $n, n' = 2, 3$ singlet states (as well as the first two $n = 4$ states in the ${}^1\Sigma^+$ symmetry) in the energy range between 0.25 and 150 eV/amu. We have also investigated the effect of the nonadiabatic rotational couplings on the charge-transfer cross sections. All the cross sections are not presented in this article, but they are available as supplementary material [37].

We have found that our method is adapted when the rotational couplings are neglected but is problematic at energies higher than 10 eV/amu when the rotational couplings are included, due to very long computational times.

We have found a strong dependence of the state-to-state charge-transfer cross sections on the principal and orbital quantum numbers, n and l , of the hydrogen atom. We observed

that the rotational couplings have an influence on the cross sections even at low energies but that their effect increases with n : for $n = 2$ states, we found that the effect of the couplings starts to be important at energies higher than about 5 eV/amu, while for the $n = 3$ states, they modify the cross sections even at energies below 1 eV/amu. However, the total cross sections are not modified by the inclusion of rotational couplings at energies below 10 eV/amu. The effect of these couplings should therefore be investigated at intermediate energies using other approaches, such as an eikonal method.

ACKNOWLEDGMENTS

The authors would like to thank G. Destrée and J.M. Teuler for their help with computational issues. J.L. acknowledges the financial support of the FRIA. This work was supported by the Fonds National de la Recherche Scientifique (IISN projects) and by the Action de Recherche Concertée ATMOS de la Communauté Française de Belgique. The financial support by the FNRS of the University of Liège Nic2 and Nic3 projects is gratefully acknowledged. We appreciate the support of COST Action CM0702 CUSPFEL. K.S. would like to thank the University of Paris-Sud 11 for financial support (N:2238).

-
- [1] H. S. W. Massey and R. A. Smith, *Proc. R. Soc. A* **142**, 142 (1933).
- [2] T. A. Green, H. I. Stanley, and Y. C. Chiang, *Helv. Phys. Acta* **38**, 109 (1965).
- [3] B. H. Bransden and L. T. Sin Fai Lam, *Proc. Phys. Soc.* **87**, 653 (1966).
- [4] L. T. Sin Fai Lam, *Proc. Phys. Soc.* **92**, 67 (1967).
- [5] R. K. Colegrave and D. B. L. Stephens, *J. Phys. B* **1**, 856 (1968).
- [6] T. G. Winter and C. C. Lin, *Phys. Rev. A* **10**, 2141 (1974).
- [7] M. Kimura, *Phys. Rev. A* **31**, 2158 (1985).
- [8] M. Kimura and C. D. Lin, *Phys. Rev. A* **34**, 176 (1986).
- [9] A. Jain, C. D. Lin, and W. Fritsch, *Phys. Rev. A* **36**, 2041 (1987).
- [10] W. Fritsch and C. D. Lin, *Phys. Rev. Lett.* **61**, 690 (1988).
- [11] M. B. Shah, P. McCallion, and H. B. Gilbody, *J. Phys. B* **22**, 3037 (1989).
- [12] H. A. Slim, E. L. Heck, B. H. Bransden, and D. R. Flower, *J. Phys. B* **23**, L611 (1990).
- [13] H. A. Slim, E. L. Heck, B. H. Bransden, and D. R. Flower, *J. Phys. B* **24**, 1683 (1991).
- [14] D. Jackson, H. A. Slim, B. H. Bransden, and D. R. Flower, *J. Phys. B* **25**, L127 (1992).
- [15] R. Shingal and C. D. Lin, *J. Phys. B* **24**, 963 (1991).
- [16] M. Terao, C. Harel, A. Salin, and R. J. Allan, *Z. Phys. D* **7**, 319 (1988).
- [17] M. H. Cherkani, S. Szucs, M. Terao, H. Hus, and F. Brouillard, *J. Phys. B* **24**, 209 (1991).
- [18] M. I. Chibisov, R. K. Janev, X. Urbain, and F. Brouillard, *J. Phys. B* **34**, 2631 (2001).
- [19] M. I. Chibisov, R. K. Janev, X. Urbain, and F. Brouillard, *J. Phys. B* **35**, 5081 (2002).
- [20] F. B. Rosmej, R. Stamm, and V. S. Lisitsa, *Europhys. Lett.* **73**, 342 (2006).
- [21] N. Vaeck, M. Desouter-Lecomte, and J. Liévin, *J. Phys. B* **32**, 409 (1999).
- [22] N. Vaeck, M.-C. Bacchus-Montabonel, E. Baloitcha, and M. Desouter-Lecomte, *Phys. Rev. A* **63**, 042704 (2001).
- [23] H. Lefebvre-Brion and R. W. Field, *The Spectra and Dynamics of Diatomic Molecules* (Elsevier Academic Press, Amsterdam, 2004).
- [24] H.-J. Werner *et al.*, MOLPRO, version 2006.1 (2006); see [<http://www.molpro.net>].
- [25] T. H. Dunning, *J. Chem. Phys.* **90**, 1007 (1989).
- [26] J. Loreau, J. Liévin, P. Palmeri, P. Quinet, and N. Vaeck, *J. Phys. B* **43**, 065101 (2010).
- [27] F. T. Smith, *Phys. Rev.* **179**, 111 (1969).
- [28] C. Zhu and H. Nakamura, *J. Chem. Phys.* **106**, 2599 (1997).
- [29] K. Sodoga, J. Loreau, D. Lauvergnat, Y. Justum, N. Vaeck, and M. Desouter-Lecomte, *Phys. Rev. A* **80**, 033417 (2009).
- [30] A. K. Belyaev, D. Egorova, J. Grosser, and T. Menzel, *Phys. Rev. A* **64**, 052701 (2001).
- [31] A. K. Belyaev, A. Dalgarno, and R. McCarroll, *J. Chem. Phys.* **116**, 5395 (2002).
- [32] M. S. Child, *Molecular Collision Theory* (Academic Press, New York, 1974).
- [33] J. A. Fleck Jr., J. R. Morris, and M. D. Feit, *Appl. Phys.* **10**, 129 (1982).
- [34] A. Jäckle and H.-D. Meyer, *J. Chem. Phys.* **105**, 6778 (1996).
- [35] E. Baloitcha, M. Desouter-Lecomte, M.-C. Bacchus-Montabonel, and N. Vaeck, *J. Chem. Phys.* **114**, 8741 (2001).
- [36] M. A. Morrison and A. N. Feldt, *Am. J. Phys.* **75**, 67 (2007).
- [37] See supplementary material at [<http://link.aps.org/supplemental/10.1103/PhysRevA.82.012708>].